Nuclear Instruments and Methods in Physics Research B 369 (2016) 95–97

Contents lists available at ScienceDirect

Nuclear Instruments and Methods in Physics Research B

journal homepage: www.elsevier.com/locate/nimb

Transit time spreads in biased paracentric hemispherical deflection analyzers

Omer Sise [a,*], Theo J.M. Zouros [b,c]

[a] Dept. of Science Education, Faculty of Education, Suleyman Demirel Univ., 32260 Isparta, Turkey
[b] Dept. of Physics, Univ. of Crete, P.O. Box 2208, GR 71003 Heraklion, Greece
[c] Tandem Lab, INPP, NCSR Demokritos, P.O. Box 60228, GR 15310 Ag. Paraskevi, Greece

ARTICLE INFO

Article history:
Received 22 June 2015
Accepted 17 September 2015
Available online 30 September 2015

Keywords:
Time-of-flight
Hemispherical deflection analyzer
Energy resolution
Time resolution

ABSTRACT

The biased paracentric hemispherical deflection analyzers (HDAs) are an alternative to conventional (centric) HDAs maintaining greater dispersion, lower angular aberrations, and hence better energy resolution without the use of any additional fringing field correctors. In the present work, the transit time spread of the biased paracentric HDA is computed over a wide range of analyzer parameters. The combination of high energy resolution with good time resolution and simplicity of design makes the biased paracentric analyzers very promising for both coincidence and singles spectroscopy applications.

1. Introduction

The hemispherical deflection analyzer (HDA) with single- or multi-channel detection has been widely used to collect electron spectra in atomic collisions – see Refs. [1,2] and references therein. For most of electron spectroscopy and spectroscopic imaging applications, the relative energy resolution of an HDA, $\Delta E/E$, is an important consideration. However, if an HDA is used to simultaneously record the position and travel time of electrons [3], or if it is used in coincidence experiments, such as in (e, $2e$) measurements [4], the time-of-flight (TOF) distribution of the arriving particles will also be important.

Motivation for the computation of flight times in HDAs has been provided by various publications as for example Imhof et a1. [5], Caprari [6], Kugeler et al. [7], and Shavorskiy et al. [3]. These studies have predicted the transit time using an approximate model, which ignores fringing fields at the boundaries. Suggestions to improve the time resolution in coincidence experiments have been made by Volkel and Sandner [4], and it has been shown that for conventional (e, 2e) spectrometers the temporal resolution is mostly defined by the time spread within the analyzer, which is usually in the nanosecond time range. An extensive study of HDAs employing elliptical trajectories applicable to paracentric HDAs including basic timing properties has been given by Zouros and Benis [1].

Imhof et al. [5] evaluated the variation of the time spread Δt as a function of pass energy E_0 and showed that it is inversely proportional to the square root of the pass energy, i.e., $\Delta t \propto E_0^{-1/2}$, assuming that both the initial angular and spatial distributions are kept constant. This means that the reduction of the time-of-flight spread for the trajectories within the analyzer can only be achieved by increasing the pass energy. However, an increase of the pass energy will lead to a decrease in the energy resolution. Therefore, a suitable compromise between good energy resolution (favoring smaller E_0) and good time resolution (favoring larger E_0) is clearly needed.

Recently, we have presented a systematic study on the transit time spread of biased paracentric HDAs [8]. Although the dominant contribution to the TOF spread is acquired within the HDA, the injection lens system indirectly affects the time spread of the analyzer to a significant extent by inducing a strong dependence of the angular spread of the electron trajectories entering the hemisphere on the pre-retardation ratio F. The angular and spatial distributions are controlled by the lens linear M_L and angular M_α magnifications constrained by the Helmholtz–Lagrange law, i.e., $|M_L||M_\alpha| = \sqrt{F}$. Zouros and Benis [9] showed that the energy resolution becomes a function of M_L and has a minimum at the optimal magnification M_{Lopt}.

In the present work, the correlation between the pre-retardation ratio F and the time and energy spread, Δt and ΔE, respectively, is evaluated by means of computer-based finite-difference trajectory simulations using SIMION 8.1 [10]. We

* Corresponding author.
E-mail address: omersise@sdu.edu.tr (O. Sise).

http://dx.doi.org/10.1016/j.nimb.2015.09.050
0168-583X/

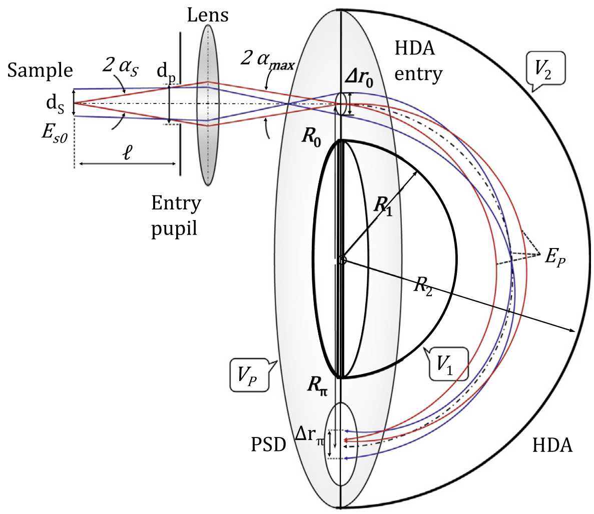

Fig. 1. Schematic of a biased paracentric HDA consisting of two concentric hemispheres of radii R_1 and R_2 equipped with an electrostatic lens and a position sensitive detector. The electron energy is the same for all trajectories, originating from an extended source. The central trajectory (black dashed-dot line) starts at $r = R_0$ and exits at $r = R_\pi$, moving on Kepler-type elliptical trajectories inside the HDA. The incident beam spot (d_S), has a maximum outgoing angle of α_S restricted by the pupil as defined by the lens entrance aperture (d_p). The decelerating lens slows the electrons and focuses them to an effective virtual aperture size (Δr_0).

assume that the virtual aperture size Δr_0 and the ingoing electron angular spread α_{max} are obtained using the optimal linear and angular magnification [9].

2. Theory and simulation

The analytical solution of the equation of motion is well documented in the extensive literature on the ideal HDA (see Ref. [1], and references therein). Here, we only give a brief introduction to the electron optical properties and time-of-flight calculations for the biased paracentric HDA. Eqs. (1)–(3) discussed below are taken from Refs. [1,8]. The analyzer consists of two concentric hemispherical electrodes of radii R_1 and R_2 equipped with an electrostatic input lens and a position sensitive detector, as shown in Fig. 1. The lens system is typically used to collimate and focus the source onto the virtual entry aperture of the HDA. Electrons entering the hemispherical field at the virtual aperture with an angular spread α_{max} with respect to the optical axis for the pass energy E_0 of the analyzer are transferred to the exit plane. In an ideal HDA (no fringing fields) a particle of charge q and energy E enters with radius r_0 and pencil angle α within an aperture of diameter Δr_0 centered at R_0, follows an elliptical trajectory and exits at r_π after going around an orbit of 180°. The central trajectory (black dashed-dot line) is defined by a particle which enters with energy E_0 at $r_0 = R_0$ with $\alpha = 0°$ and exits at $r_\pi = R_\pi$. An exit aperture is typically placed with center at R_π. Alternatively a position sensitive detector is used at the exit. The most well-known (conventional) arrangement utilizes, $R_0 = R_\pi = (R_1 + R_2)/2$, the mean radius or central radius of the HDA (and therefore referred to as the centric position entry), in which case the central trajectory is a circle.

The electron trajectories in an ideal HDA potential of the form $V(r) = -k/r + c$ are described by Kepler orbits. The non-relativistic elliptical trajectories within the radial $1/r$ potential have been derived in detail in Zouros and Benis [1]. The potentials that need to be applied to the inner and the outer hemispheres are given by

$$qV_i = E_0\left\{F - \gamma\left(\frac{R_0}{R_\pi}\right)\left[\frac{R_0 + R_\pi}{R_i} - 1\right]\right\} \quad (i = 1, 2) \tag{1}$$

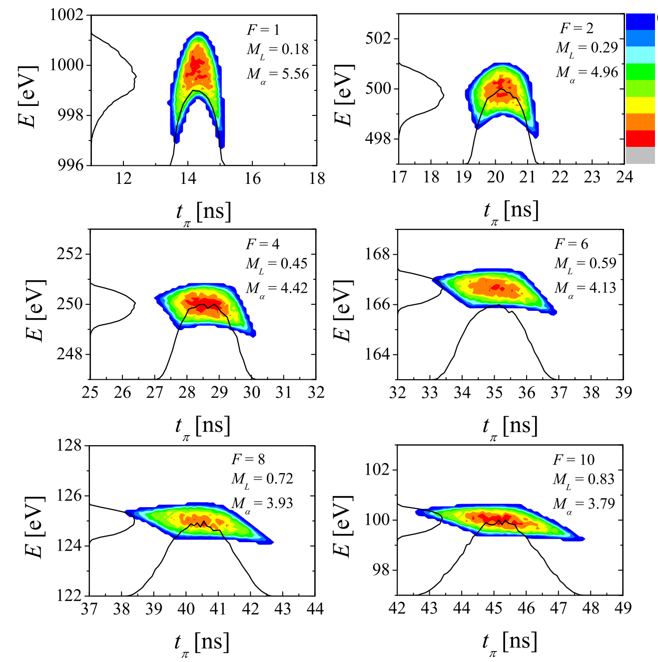

Fig. 2. Calculated time and energy distributions at the exit of the HDA for six different values of $F = 1 - 10$, for a monoenergetic beam of $E_{s0} = 1000$ eV. Simulations were performed for a source extent of $d_S = 2.5$ mm. Normalized line profiles resulting from vertical and horizontal projections of the distributions are also shown. The detector plane is assumed to coincide with the HDA exit plane.

where F is the pre-retardation ratio E_{s0}/E_0, and E_{s0} is the electron source energy. The parameter γ, known as the entry biasing parameter is related to the entry bias V_0, the nominal potential at the entry at R_0, given by $qV_0 = (F - \gamma)E_0$ [1].

As shown in Fig. 1, the electron entering the HDA with a small angle α follows an elliptical trajectory in the radial electrostatic field. Due to the different conditions of their trajectories, a spread in the transit times also accrues. Neglecting the fringing fields at the boundaries and other mechanical imperfections, the transit times, t_π, of the particles through the analyzer are given by [8]

$$t_\pi = \frac{T_0}{2\pi}\left\{\pi + 2\arctan\left[\sin\alpha\sqrt{\left(-1 + \frac{2}{\rho_0}\right)}\right] - \frac{4\left(\sqrt{\frac{\rho_0}{2-\rho_0}}\right)\sin\alpha}{\cos 2\alpha - \left(\frac{2+\rho_0}{2-\rho_0}\right)}\right\} \tag{2}$$

where T_0 is the period of the full Kepler orbit given by $T_0 = 2\pi\sqrt{ma^3/qk}$, and $\rho_0 = r_0/a$. Here, $a = -qk/(2E_{tot})$ is the semi-major axis, E_{tot} is the conserved total energy, and $k = R_1 R_2 (V_2 - V_1)/(R_2 - R_1)$. From Eq. (2), one can see that the sign of α affects the value of t_π. In other words, the time-of-flight of a trajectory starting with angle $-\alpha$ is not identical to that starting with $+\alpha$.

In the presence of fringing fields the flight time cannot be established in a simple analytical form. Thus, the calculations have to be carried out numerically.

In Ref. [9] it has been shown that the linear magnification of the lens can be chosen so that it minimizes the expression of the energy resolution. The Helmholtz–Lagrange principle has been applied to find the optimal base width energy resolution as a function of the optimal lens magnification between conjugate lens object-image points. Using $\Delta r_0 = |M_L| d_S$ and $\alpha_{max} = M_L d_p/(\sqrt{F}2\ell)$, the optimal lens magnification M_{Lopt} can be written by the formula [9]:

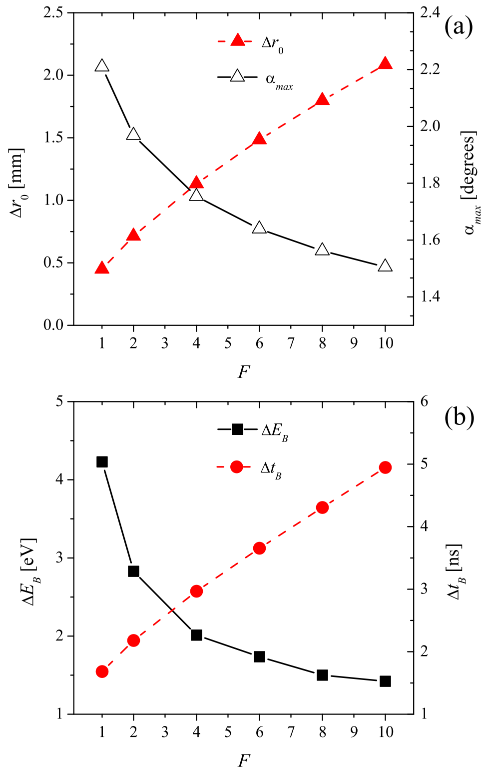

Fig. 3. (a) The values of the virtual entry aperture size Δr_0 and the angular spread α_{max} computed by the lens magnification M_L and angular magnification M_α according to the Helmholtz–Lagrange stipulations plotted as a function of F. (b) Comparison of the base energy ΔE_B and time Δt_B spread as a function of F.

$$|M_{Lopt}| = \left[\frac{1}{2}\left(\frac{FD}{d_s}\right)\left(\frac{d_p}{\ell}\right)^2\right]^{\frac{1}{3}} \quad (3)$$

where parameters d_s, d_p, ℓ are shown in Fig. 1. Here, D is the energy dispersion.

We have used the specific spectrometer parameters in the present calculation: $R_0 = 82.55$ mm, $R_1 = 72.4$ mm, $R_2 = 130.8$ mm, $\gamma = 1.5, d_S = 2.5$ mm, $d_p = 4$ mm, $\ell = 288.5$ mm.

3. Results and discussion

The changes in the transit time depend on the virtual entry size Δr_0 and the acceptance angle α_{max}. The calculated time-energy distributions for a monoenergetic input beam ($E_{s0} = 1000eV$) for six different values of the pre-retardation ratio $F = 1 - 10$ are shown in Fig. 2. For a fixed F, the linear magnification is calculated by Eq. (3) and then the angular magnification is obtained using the Helmholtz–Lagrange law. As shown in Fig. 2, the width of the time-of-flight distribution varies significantly with the angular magnification. For higher F, the time-spread increases with F, and the contour plot looks like a trapezoid.

Fig. 3(a) shows the dependence of the widths of the virtual entry aperture Δr_0 and the values of the maximum half-angle α_{max} on F. In Fig. 3(b) we show a comparison between the optimal energy and time spread values ΔE_B and Δt_B obtained by SIMION as a function of F. The energy spread is seen to drop-off with F, while Δr_0 (α_{max}) increases (decreases) with F. The relative energy resolution $\Delta E_B/E_{s0}$ ranges in values between $0.42\% - 0.14\%$ for $F = 1 - 10$, respectively. As expected, an opposite trend is observed for the time spread, ranging in values between $1.68 - 4.95$ ns for $F = 1 - 10$, respectively. Since the time-of-flight t_π increases with increasing F, the relative time resolution $\Delta t_B/t_\pi$ is almost constant and is found to be 11.08%.

4. Summary and conclusion

The time-of-flight distributions in a biased paracentric HDA for different pre-retardation ratios F have been studied. The trajectory related electron energy and time spreads were calculated numerically since neither their flight times nor their positions are predictable analytically in the fringing field of the HDA. Our analysis quantifies the effect of varying the controllable virtual aperture entry size and acceptance angle on selected output variables of energy and time spread. The present simulation demonstrates that the biased paracentric HDA offers good time distribution with relatively high energy resolution.

This research has been co-financed by the European Union (European Social Fund ESF) and Greek national funds through the Operational Program ”Education and Lifelong Learning” of the National Strategic Reference Framework (NSRF) Research Funding Program: THALES. Investing in knowledge society through the European Social Fund, Grant No. MIS 377289. The authors would like to thank David J. Manura of SIS for his help with various SIMION issues.

References

[1] T.J.M. Zouros, E.P. Benis, The hemispherical deflector analyser revisited. I. Motion in the ideal 1/r potential, generalized entry conditions, Kepler orbits and spectrometer basic equation, J. Electron Spectrosc. Relat. Phenom. 125 (3) (2002) 221–248. Erratum. In: J. Electron Spectrosc. Relat. Phenom. (142), 2005, 175–176. http://dx.doi.org/10.1016/S0368-2048(02)00137-8.

[2] E.P. Benis, T.J.M. Zouros, The hemispherical deflector analyser revisited: II. Electron-optical properties, J. Electron Spectrosc. Relat. Phenom. 163 (1–3) (2008) 28–39, http://dx.doi.org/10.1016/j.elspec.2008.02.001.

[3] A. Shavorskiy, S. Neppl, D.S. Slaughter, J.P. Cryan, K.R. Siefermann, et al., Sub-nanosecond time-resolved ambient-pressure X-ray photoelectron spectroscopy setup for pulsed and constant wave X-ray light sources, Rev. Sci. Instrum. 85 (9) (2014), http://dx.doi.org/10.1063/1.4894208 (Article ID: 093102).

[4] M. Volkel, W. Sandner, Optimisation of electron energy analysers for application in coincidence experiments, J. Phys. E: Sci. Instrum. 16 (5) (1983) 456–462, http://dx.doi.org/10.1088/0022-3735/16/5/020.

[5] R.E. Imhof, A. Adams, G.C. King, Energy and time resolution of the 180 degrees hemispherical electrostatic analyser, J. Phys. E: Sci. Instrum. 9 (2) (1976) 138–142, http://dx.doi.org/10.1088/0022-3735/9/2/024.

[6] R.S. Caprari, Exit position and transit time analysis of hemispherical electrostatic analysers, Meas. Sci. Technol. 6 (7) (1995) 1063–1064, http://dx.doi.org/10.1088/0957-0233/6/7/032.

[7] O. Kugeler, S. Marburger, U. Hergenhahn, Calculation and measurement of the time-of-flight spread in a hemispherical electron energy analyzer, Rev. Sci. Instrum. 74 (9) (2003) 3955–3961, http://dx.doi.org/10.1063/1.1599060.

[8] O. Sise, T.J.M. Zouros, Position, energy, and transit time distributions in a hemispherical deflector analyzer with position sensitive detector, J. Spectrosc. 2015 (2015) 20, http://dx.doi.org/10.1155/2015/153513 (Article ID: 153513).

[9] T.J.M. Zouros, E.P. Benis, Optimal energy resolution of a hemispherical analyzer with virtual entry, Appl. Phys. Lett. 86 (9) (2005), http://dx.doi.org/10.1063/1.1871339 (Article ID: 094105).

[10] SIMION version 8.1.2.20, Scientific Instrument Services, Inc., Ringoes, NJ, 2014, see <http://www.simion.com>.